

Free-standing graphene membranes on glass nanopores for ionic current measurements

Michael I. Walker, Robert S. Weatherup, Nicholas A. W. Bell, Stephan Hofmann, and Ulrich F. Keyser

Citation: [Applied Physics Letters](#) **106**, 023119 (2015); doi: 10.1063/1.4906236

View online: <http://dx.doi.org/10.1063/1.4906236>

View Table of Contents: <http://scitation.aip.org/content/aip/journal/apl/106/2?ver=pdfcov>

Published by the [AIP Publishing](#)

Articles you may be interested in

[Water permeability of nanoporous graphene at realistic pressures for reverse osmosis desalination](#)

J. Chem. Phys. **141**, 074704 (2014); 10.1063/1.4892638

[Electrostatic correlations on the ionic selectivity of cylindrical membrane nanopores](#)

J. Chem. Phys. **140**, 064701 (2014); 10.1063/1.4864323

[Mechanical properties of nanoporous graphene membrane](#)

J. Appl. Phys. **115**, 034303 (2014); 10.1063/1.4862312

[Fabrication of hierarchical nanostructures using free-standing trilayer membrane](#)

J. Vac. Sci. Technol. B **31**, 06FF04 (2013); 10.1116/1.4821655

[Effective large-area free-standing graphene field emitters by electrophoretic deposition](#)

Appl. Phys. Lett. **101**, 183107 (2012); 10.1063/1.4765070

The advertisement features a 3D cutaway simulation of a mechanical part with a red-to-blue color gradient. The text 'Over 600 Multiphysics Simulation Projects' is prominently displayed in white and blue. A blue button with the text 'VIEW NOW >>' is located in the bottom right corner. The COMSOL logo is positioned at the bottom right of the image.

Over **600** Multiphysics Simulation Projects

[VIEW NOW >>](#)

COMSOL

Free-standing graphene membranes on glass nanopores for ionic current measurements

Michael I. Walker,¹ Robert S. Weatherup,² Nicholas A. W. Bell,¹ Stephan Hofmann,² and Ulrich F. Keyser^{1,a)}

¹*Cavendish Laboratory, University of Cambridge, J.J. Thomson Avenue, Cambridge CB3 0HE, United Kingdom*

²*Department of Engineering, University of Cambridge, Cambridge CB3 0FA, United Kingdom*

(Received 11 November 2014; accepted 2 January 2015; published online 16 January 2015)

A method is established to reliably suspend graphene monolayers across glass nanopores as a simple, low cost platform to study ionic transport through graphene membranes. We systematically show that the graphene seals glass nanopore openings with areas ranging from 180 nm² to 20 μm², allowing detailed measurements of ionic current and transport through graphene. In combination with *in situ* Raman spectroscopy, we characterise the defects formed in ozone treated graphene, confirming an increase in ionic current flow with defect density. This highlights the potential of our method for studying single molecule sensing and filtration. © 2015 AIP Publishing LLC.

[<http://dx.doi.org/10.1063/1.4906236>]

There is great potential for graphene monolayers in micro and nano fluidics.¹ Graphene's mechanical strength enables free standing atomically thin membranes² and theoretical approaches suggest these could, with appropriate pores, exhibit high performance, size selective filtration.^{3,4} Applications for graphene membranes include molecular sieving, water filtration, and desalination.^{5,6} Progress has been made towards achieving this in studies of nanoporous sheets of graphene that have been shown to filter by size of molecule for both gases⁷ and ionic solutions.⁸ Porous graphene has been created by using ion/electron beam etching,⁹ exposure to UV light and ozone,¹⁰ or oxidative etching.¹¹

Free standing graphene membranes can be studied by placing the graphene on a porous substrate, where much of the graphene is supported.⁸ Alternatively, MEMS fabrication techniques are used to suspend isolated areas, up to ~50 μm², of graphene but often involve many processing steps.^{10,12,13} Here, we present a simple technique to expedite the study of free standing graphene membranes separating two liquid reservoirs by combining them with glass nanopores in a hybrid system. Glass nanopores formed by pulling hollow glass capillaries, heated at the center by a laser, so that they taper to a fine tip were developed for use in patch clamp experiments but have found uses in a wide range of fields.¹⁴ They provide a robust and cheap platform for studying flexible membranes such as lipid bilayers¹⁵ and DNA origami nanopores.¹⁶ The diameter of the nanopore, which is determined by the pulling parameters, can range from tens of nanometers to a few microns.

In this paper, we demonstrate a straightforward method to suspend graphene monolayers across glass nanopores as a rapid and reliable means to manipulate and study graphene membranes. The graphene seals the tip, significantly reducing the ionic current flow into the glass nanopore. We show that the measured ionic current flow is due to current flow through the membrane and demonstrate that we can detect the extent of defects in ozone damaged graphene. We

quantify the effect of the ozone treatment by measurements of ionic transport and Raman spectroscopy.

Figure 1(a) shows the setup used to place graphene on the tip of a glass nanopore by pushing it vertically into a graphene monolayer floating on the surface of a reservoir (Figure 1(b)). The glass capillary, filled with an aqueous solution of 1M NaCl, is mounted on a micromanipulator (*Scientifica, Patch Star*) positioned above a custom made inverted microscope which images the water surface to acquire *in situ* Raman spectra. The reservoir is mounted on a purpose built x, y, z translation stage and Ag/AgCl electrodes in the capillary and reservoir are connected to an amplifier (*Axopatch 200B*). LabVIEW software (*National Instruments, 2009*) is used to control the micromanipulator, apply voltages, and record all measurements. The micromanipulator is used to position the nanopore above the graphene and lower it down whilst the current between the two electrodes is monitored. Contact between the glass nanopore and the graphene is detected when the current increases and the drive down of the nanopore is stopped. A typical drive down and retraction trace is shown in Figure 1(c).

We form nanopores by pulling glass capillaries (*Sutter and Hilgenberg GmbH*) using a laser-based capillary puller (*Sutter P2000*) as described before.¹⁷ In this work, nanopores from five different pulling programs are used with diameters from 15 nm to 5 μm (further details in supplementary material¹⁸).

Graphene is grown by chemical vapour deposition (CVD), in a custom built cold wall reactor, using 25 μm thick platinum foil (*Alfa Aesar, 99.99%*) as the catalyst and C₂H₄ as the precursor^{19–22} (details in supplementary material¹⁸). The CVD grown graphene is polycrystalline with large grain sizes of 20–100 μm, as confirmed by scanning electron microscopy of a sample for which growth was interrupted prior to complete coverage. It is transferred by spin coating a polymer (*polymethylmethacrylate, 4 wt. % in anisole, 950k molecular weight*) on to the surface and releasing the graphene from the catalyst by an electrolysis-based bubbling technique.^{20,23,24} The polymer supported graphene is floated on an aqueous solution saturated with NaCl, allowing it to be lifted out onto the

^{a)}ufk20@cam.ac.uk

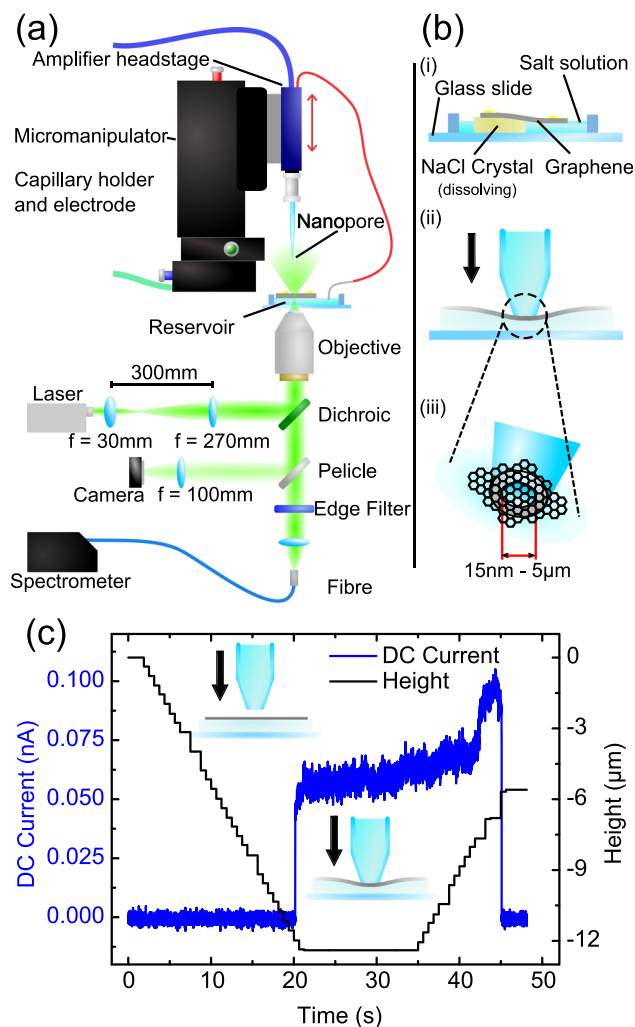


FIG. 1. (a) Diagram of the experimental setup showing the nanopore mounted on a micromanipulator and *in situ* Raman spectrometer. (b) (i) Graphene is floated by dissolving a salt crystal into a reservoir. (ii) The graphene is then sealed onto the nanopore. (iii) This places a graphene monolayer across the tip of the glass nanopore. (c) Current and nanopore height traces for a typical drive down and seal onto a graphene membrane floating on 1M NaCl, with a 400 nm glass nanopore and 10 mV bias. When the nanopore lands on the graphene membrane, the current increases and the computer controlled drive down stops. The nanopore is then lifted up away from the surface until the current returns to the initial value.

surface of a cleaved single crystal of NaCl (*SPI-Chem*), without significant dissolution of the substrate. The sample is then dried at $\sim 50^\circ\text{C}$, and the polymer dissolved by immersion in acetone. Finally Au, with a thickness of 30 nm, is thermally evaporated through a shadow mask to form thin stripes on the graphene to aid locating the membranes in our inverted microscope. The graphene is floated on the surface of the liquid by placing the salt crystal into the reservoir and allowing it to dissolve to yield a 1M NaCl solution. The reservoir is a microfluidic cell designed to limit evaporation, whilst ensuring a thin film of water (100–200 μm) to facilitate imaging.

The inverted microscope is used to find, verify, and characterise the graphene on the nanopore at the tip of the capillary by *in situ* Raman spectroscopy. The objective (*Olympus ACHN 40XP*) is used to focus a 532 nm laser (*Laser Quantum Gem, CW, 532 nm, 100 mW*) onto the graphene. The reflected light is separated using a dichroic mirror (*Semrock 532 nm RazorEdge*), filtered using an edge filter (*Semrock 532 nm*

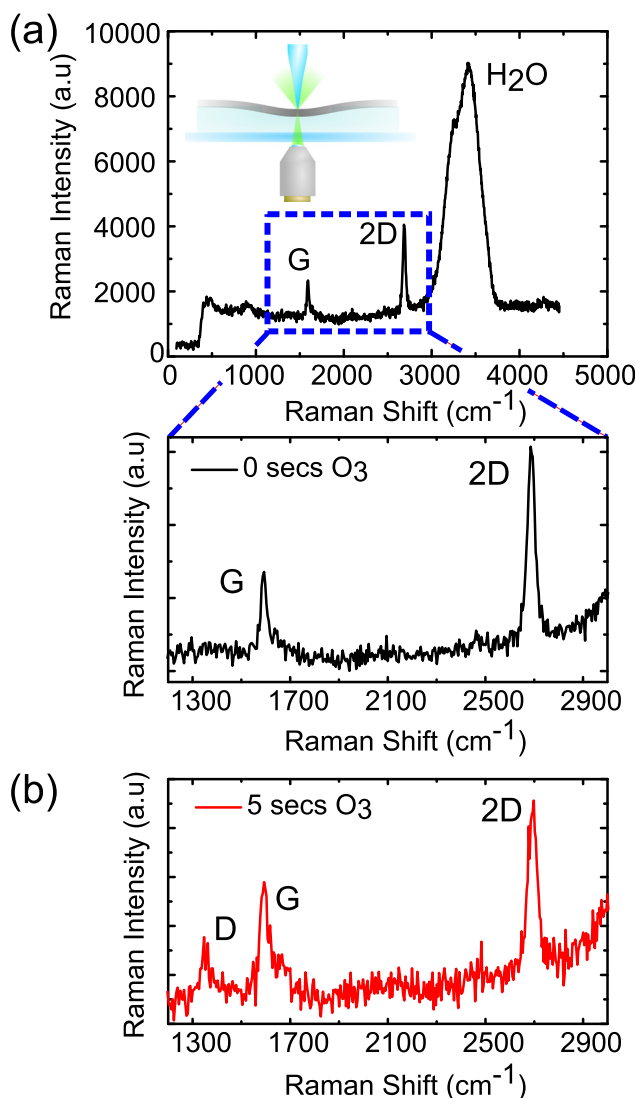


FIG. 2. (a) Raman spectra obtained from as grown graphene floating on water showing a large peak due to the water and background from the glass slide. The magnified section of the spectrum shows the characteristic Raman spectrum of graphene. The ratio of the indicated G to 2D peaks indicates monolayer and the absence of a D peak indicates a low defect density. (b) Typical Raman spectrum from ozone damaged graphene floating on water. The D peak is clearly visible after the sample was exposed to ozone for 5 s.

EdgeBasic), and the resulting spectra measured (*Ocean Optics, Ventanna 532 nm*). The microscope allows the graphene to be found on the surface of the reservoir, first by optically locating gold strips and then focusing the laser onto the adjacent graphene to record a Raman spectrum.

We can characterise the quality of graphene sheets floating on the water surface. A typical Raman spectrum for a graphene membrane floating on the surface of the reservoir is shown in Figure 2(a). The two main graphene peaks are clearly visible at $\sim 1600\text{ cm}^{-1}$ (G Peak) and $\sim 2690\text{ cm}^{-1}$ (2D Peak),²⁵ and there is a significant peak from the water corresponding to OH stretching modes ($3000\text{--}4000\text{ cm}^{-1}$).²⁶ We are not able to resolve any significant differences between the Raman spectra of graphene floating on water compared to graphene which has been transferred on to SiO_2 .

To show that we can detect graphene properties such as defect density, we investigated ozone damaged graphene.

Graphene samples were damaged by exposing them to ozone for 5–20 s (Ref. 27) (details in supplementary material¹⁸). The damaged graphene is distinguished in Raman spectroscopy by the growth of the D peak ($\sim 1350\text{ cm}^{-1}$), indicating the presence of defects.²⁸ Figure 2(b) shows a typical Raman spectrum on water after 5 s ozone treatment; further treatment causes the D peak to increase and subsequently the 2D to G peak ratio to decrease (data not shown).²⁹

To apply our method to assess membrane quality, we must first verify that the observed current is due to transport through the graphene. The inset of Figure 3(a) shows a schematic illustration of the proposed ionic current flow through the graphene membrane (red arrow) and the alternative route around the perimeter of the nanopore (green arrows). We evaluate the ionic current through the graphene membrane by recording an I-V curve and investigate the variation when using different sizes of glass nanopore. Before each experiment, we determine the resistance of the bare nanopore in solution and then seal it on to a graphene membrane (example in supplementary material¹⁸). A reduction in current, compared to the bare nanopore, indicates that the graphene has sealed across the tip of the nanopore. The sealed resistances range from 1–2 G Ω for 15 nm nanopores to 1–10 M Ω for 5 μm nanopores, although we note that these resistances are lower than other published values.¹² We observe a linear relationship between the sealed and bare resistances on as

grown graphene (Figure 3(a)). As the resistance of the bare nanopore is inversely proportional to its area, it follows that the sealed resistance scales with the area of the graphene on the tip. We can therefore conclude that the primary conduction route is through the graphene membrane. Given that a single crystal graphene membrane is expected to be impermeable,^{30,31} we attribute the current observed to intrinsic defects in the CVD grown graphene and assume that there is no ongoing charge transfer to the graphene. The graphene domain sizes are larger than our glass nanopores, but it is likely that a proportion of the measurements with the larger diameters will capture grain boundaries contributing to the variation we observe in sealed resistances.

In order to demonstrate that our method can indeed detect ionic transport through damaged samples, we analysed the ozone treated samples described above. Figure 3(b) shows that the resistance of the damaged graphene membranes decreases compared to the as grown sample, but the linear dependence with the bare nanopore resistance remains. The slightly non-linear relationship between sealed and bare resistances for graphene damaged with ozone for 5 s is an indication that the induced defects are more widely spaced than the size of the smallest glass nanopore. This means that the smallest nanopores may seal onto an area of graphene which has not been affected by the ozone treatment. With increased ozone exposure time, the number of defects is

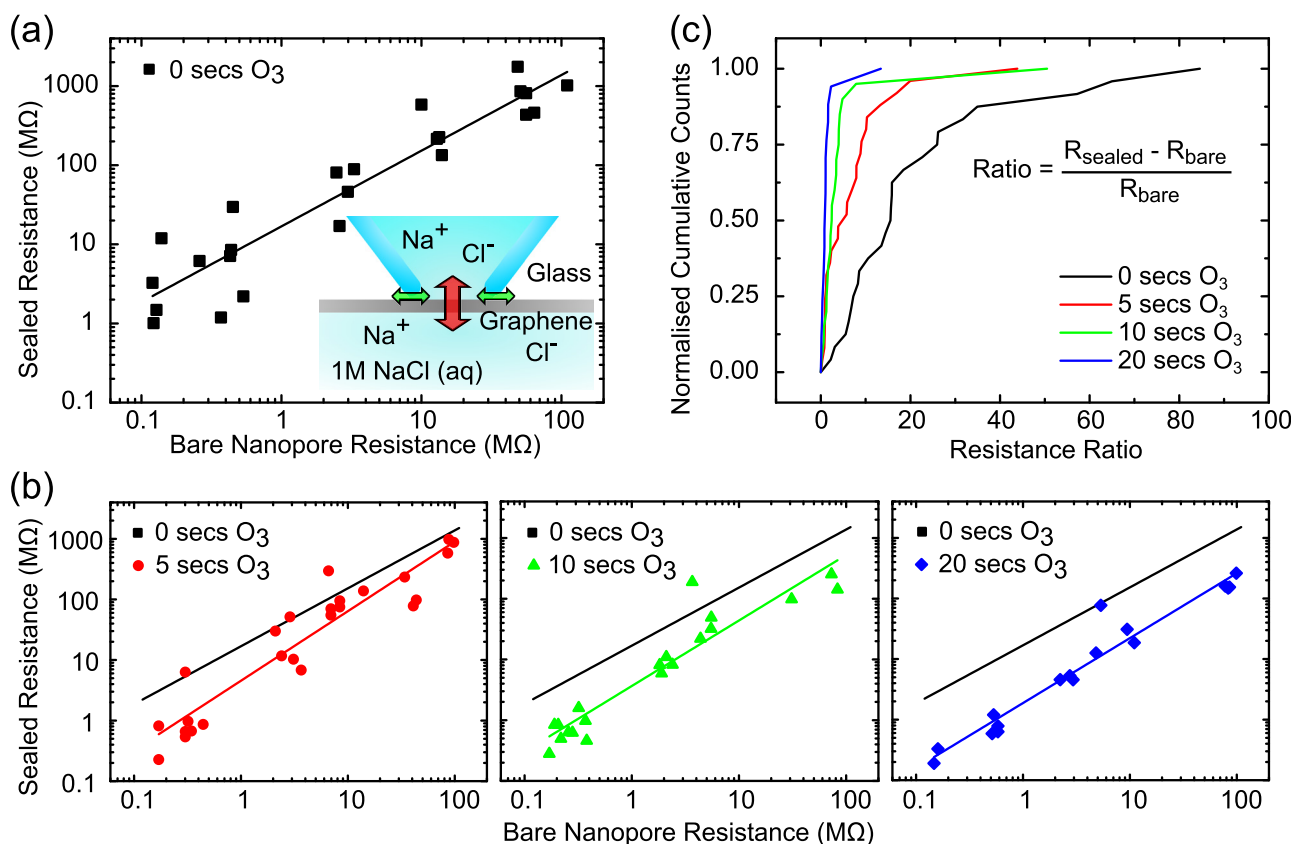


FIG. 3. (a) Resistance of nanopores sealed on as grown graphene plotted against the bare nanopore resistance. The gradient of the fitted line is 0.957 ± 0.075 . This shows that the sealed resistance is directly proportional to the bare resistance and hence proportional to the area, indicating that the current measured is due to transport through the graphene. (Inset) Schematic of nanopore-graphene interface showing possible current routes through the graphene membrane (red arrow) or around the perimeter (green arrows). (b) Resistance of nanopores sealed on to graphene damaged by exposure to ozone. The fit to as grown samples is shown on each graph for comparison. For 5 s O_3 exposure, the gradient of the fit is 1.15 ± 0.087 , for 10 s O_3 the gradient is 1.08 ± 0.091 , and for 20 s O_3 the gradient is 1.07 ± 0.066 . (c) Plot of cumulative resistance ratio $(R_{\text{sealed}} - R_{\text{bare}})/R_{\text{bare}}$ normalised to number of experiments for each of the graphene samples. This ratio is independent of the area. The resistance of the graphene membranes decreases with ozone damage.

sufficiently high that all of the nanopores sample the defect distribution evenly, so the sealed resistances are inversely proportional to the area of graphene. The ratio between the sealed resistance and the bare resistance is a measure of the resistance of the graphene membrane independent of the area. Cumulative counts of this ratio for all of the experiments illustrate how the resistance of the graphene decreases with ozone treatment (Figure 3(c)). The effect of the ozone induced defects is visible in the both the Raman spectra and the electrical characterisation where we see that the defects provide additional routes for ionic transport.

We can assess the defect density of our graphene sheets by estimating the area through which ionic current is flowing. For this, we calculated an effective total defect area directly from the resistance, assuming that the thickness of the graphene layer is 0.6 nm.¹² This gives an average defect area for a graphene membrane suspended across 180 nm² (15 nm diameter) pores of 0.11 nm², equivalent to a single defect with a diameter of 0.38 nm. Under the assumption that only one defect is captured by the 180 nm² pore, we can use this defect size to calculate the defect density for our as grown and damaged graphene samples from the measurements using the larger nanopores. This assumption is supported by the non-linearity we observe and this defect size corresponds with typical values from the literature.¹¹ We find that the average defect density in our as-grown graphene is $8 \times 10^9 \text{ cm}^{-2}$, increasing to $5 \times 10^{11} \text{ cm}^{-2}$ in the sample which has been exposed to ozone for 20 s. This assumes that ozone treatment induces new defects in preference to enlarging existing defects. These values are comparable to defect densities measured for CVD grown graphene¹¹ and consistent with the defect densities extracted from our measurements of the Raman D peak intensity.²⁹

We propose to use this platform to investigate the transport of different molecules through graphene monolayers incorporating defects and pores. Developing methods to control pore sizes and distribution will allow selective filters to be investigated. Another promising application for graphene membranes is nanopore sensing.³² Nanopores in graphene membranes formed by TEM drilling^{10,12,13} have been demonstrated for single molecule sensing and could result in high resolution for use in DNA sequencing.³³ Our technique will facilitate studies of pore formation and translocations of single molecules for nanopore sensing.

We have demonstrated a method for sealing graphene on the tips of glass nanopores with simultaneous, *in situ* characterisation by Raman spectroscopy. Varying the glass nanopore area has shown that our approach measures the ionic current flow through graphene membranes. Applying our technique to ozone damaged graphene has allowed us to study the effect of defects on ionic transport. Our method enables further studies of transport through graphene membranes for filtration and sensing applications.

The authors would like to thank S. Purushothaman and K. Göpfrich for careful reading of the manuscript and V. Thacker for useful discussions. This work was supported by the

EPSRC Cambridge NanoDTC, EP/G037221/1, and EPSRC grant GRAPHTED, EP/K016636/1. R.S.W. acknowledges a Research Fellowship from St. John's College, Cambridge. N.A.W.B. acknowledges an EPSRC doctoral prize award.

- ¹A. K. Geim, *Science* **324**, 1530 (2009).
- ²C. Lee, X. Wei, J. W. Kysar, and J. Hone, *Science* **321**, 385 (2008).
- ³D. Jiang, V. R. Cooper, and S. Dai, *Nano Lett.* **9**, 4019 (2009).
- ⁴K. Sint, B. Wang, and P. Král, *J. Am. Chem. Soc.* **130**, 16448 (2008).
- ⁵D. Cohen-Tanugi and J. C. Grossman, *Nano Lett.* **12**, 3602 (2012).
- ⁶M. E. Suk and N. R. Aluru, *J. Phys. Chem. Lett.* **1**, 1590 (2010).
- ⁷S. P. Koenig, L. Wang, J. Pellegrino, and J. S. Bunch, *Nat. Nanotechnol.* **7**, 728 (2012).
- ⁸S. C. O'Hern, C. A. Stewart, M. S. H. Boutilier, J.-C. Idrobo, S. Bhaviripudi, S. K. Das, J. Kong, T. Laoui, M. Atieh, and R. Karnik, *ACS Nano* **6**, 10130 (2012).
- ⁹C. J. Russo and J. A. Golovchenko, *Proc. Natl. Acad. Sci. U. S. A.* **109**, 5953 (2012).
- ¹⁰C. A. Merchant, K. Healy, M. Wanunu, V. Ray, N. Peterman, J. Bartel, M. D. Fischbein, K. Venta, Z. Luo, A. T. C. Johnson, and M. Drndić, *Nano Lett.* **10**, 2915 (2010).
- ¹¹S. C. O'Hern, M. S. H. Boutilier, J.-C. Idrobo, Y. Song, J. Kong, T. Laoui, M. Atieh, and R. Karnik, *Nano Lett.* **14**, 1234 (2014).
- ¹²S. Garaj, W. Hubbard, A. Reina, J. Kong, D. Branton, and J. A. Golovchenko, *Nature* **467**, 190 (2010).
- ¹³G. F. Schneider, S. W. Kowalczyk, V. E. Calado, G. Pandraud, H. W. Zandbergen, L. M. K. Vandersypen, and C. Dekker, *Nano Lett.* **10**, 3163 (2010).
- ¹⁴C. A. Morris, A. K. Friedman, and L. A. Baker, *Analyst* **135**, 2190 (2010).
- ¹⁵S. Hernández-Ainsa, C. Muus, N. A. W. Bell, L. J. Steinbock, V. V. Thacker, and U. F. Keyser, *Analyst* **138**, 104 (2013).
- ¹⁶N. A. W. Bell, V. V. Thacker, S. Hernández-Ainsa, M. E. Fuentes-Perez, F. Moreno-Herrero, T. Liedl, and U. F. Keyser, *Lab Chip* **13**, 1859 (2013).
- ¹⁷L. J. Steinbock, O. Otto, C. Chimere, J. Gornall, and U. F. Keyser, *Nano Lett.* **10**, 2493 (2010).
- ¹⁸See supplementary material at <http://dx.doi.org/10.1063/1.4906236> for details of the glass nanopores used and further details of the graphene growth process, ozone treatment, and typical IV curves.
- ¹⁹R. S. Weatherup, B. C. Bayer, R. Blume, C. Ducati, C. Baetz, R. Schlögl, and S. Hofmann, *Nano Lett.* **11**, 4154 (2011).
- ²⁰R. S. Weatherup, B. Dlubak, and S. Hofmann, *ACS Nano* **6**, 9996 (2012).
- ²¹P. R. Kidambi, C. Ducati, B. Dlubak, D. Gardiner, R. S. Weatherup, M.-B. Martin, P. Seneor, H. Coles, and S. Hofmann, *J. Phys. Chem. C* **116**, 22492 (2012).
- ²²R. S. Weatherup, H. Amara, R. Blume, B. Dlubak, B. C. Bayer, M. Diarra, M. Bahri, A. Cabrero-Vilatela, S. Caneva, P. R. Kidambi, M.-B. Martin, C. Deranlot, P. Seneor, R. Schloegl, F. Ducastelle, C. Bichara, and S. Hofmann, *J. Am. Chem. Soc.* **136**, 13698 (2014).
- ²³Y. Wang, Y. Zheng, X. Xu, E. Dubuisson, Q. Bao, J. Lu, and K. P. Loh, *ACS Nano* **5**, 9927 (2011).
- ²⁴R. S. Weatherup, C. Baetz, B. Dlubak, B. C. Bayer, P. R. Kidambi, R. Blume, R. Schloegl, and S. Hofmann, *Nano Lett.* **13**, 4624 (2013).
- ²⁵A. C. Ferrari and D. M. Basko, *Nat. Nanotechnol.* **8**, 235 (2013).
- ²⁶Y. Tominaga, A. Fujiwara, and Y. Amo, *Fluid Phase Equilib.* **144**, 323 (1998).
- ²⁷M.-B. Martin, B. Dlubak, R. S. Weatherup, H. Yang, C. Deranlot, K. Bouzouhane, F. Petroff, A. Anane, S. Hofmann, J. Robertson, A. Fert, and P. Seneor, *ACS Nano* **8**, 7890 (2014).
- ²⁸M. Lucchese, F. Stavale, E. M. Ferreira, C. Vilani, M. Moutinho, R. B. Capaz, C. Achete, and A. Jorio, *Carbon* **48**, 1592 (2010).
- ²⁹L. G. Cançado, A. Jorio, E. H. M. Ferreira, F. Stavale, C. A. Achete, R. B. Capaz, M. V. O. Moutinho, A. Lombardo, T. S. Kulmala, and A. C. Ferrari, *Nano Lett.* **11**, 3190 (2011).
- ³⁰V. Berry, *Carbon* **62**, 1 (2013).
- ³¹J. S. Bunch, S. S. Verbridge, J. S. Alden, A. M. van der Zande, J. M. Parpia, H. G. Craighead, and P. L. McEuen, *Nano Lett.* **8**, 2458 (2008).
- ³²J. J. Kasianowicz, E. Brandin, D. Branton, and D. W. Deamer, *Proc. Natl. Acad. Sci. U. S. A.* **93**, 13770 (1996).
- ³³D. B. Wells, M. Belkin, J. Comer, and A. Aksimentiev, *Nano Lett.* **12**, 4117 (2012).